

# Large Model driven Radiology Report Generation with Clinical Quality Reinforcement Learning

Zijian Zhou<sup>1</sup>, Miaoqing Shi<sup>2\*</sup>, Meng Wei<sup>3</sup>, Oluwatosin Alabi<sup>3</sup>, Zijie Yue<sup>2</sup>, and Tom Vercauteren<sup>3</sup>

<sup>1</sup> Department of Informatics, King's College London

<sup>2</sup> College of Electronic and Information Engineering, Tongji University

<sup>3</sup> School of Biomedical Engineering & Imaging Sciences, King's College London

**Abstract.** Radiology report generation (RRG) has attracted significant attention due to its potential to reduce the workload of radiologists. Current RRG approaches are still unsatisfactory against clinical standards. This paper introduces a novel RRG method, **LM-RRG**, that integrates large models (LMs) with clinical quality reinforcement learning to generate accurate and comprehensive chest X-ray radiology reports. Our method first designs a large language model driven feature extractor to analyze and interpret different regions of the chest X-ray image, emphasizing specific regions with medical significance. Next, based on the large model's decoder, we develop a multimodal report generator that leverages multimodal prompts from visual features and textual instruction to produce the radiology report in an auto-regressive way. Finally, to better reflect the clinical significant and insignificant errors that radiologists would normally assign in the report, we introduce a novel clinical quality reinforcement learning strategy. It utilizes the radiology report clinical quality (RadCliQ) metric as a reward function in the learning process. Extensive experiments on the MIMIC-CXR and IU-Xray datasets demonstrate the superiority of our method over the state of the art.

**Keywords:** Radiology Report Generation · Large Models · Reinforcement Learning.

## 1 Introduction

Chest X-ray radiology report generation (RRG) aims to automatically generate radiology reports based on given images, ensuring the accuracy and fluency of the reports. Since this technology could significantly reduce the time that radiologists spend on writing reports, recent advances in multimodal models have renewed the attention on RRG from both the radiology and computer science communities [4,19,26,9,6,7,24,27,14,13]. The core technique of radiology report generation stems from image captioning [21,23] in a general computer vision view. Unlike image captioning, RRG focuses on reporting the disease-related symptoms and also reasoning from these symptoms.

---

\* Corresponding author.

Given that chest X-ray images are generally similar in appearance in comparison to the diversity observed in natural images, the RRG model needs to pay close attention to their details, particularly on regions with different medical implications. To address this, some recent methods [24,6] start to extract features from specific regions of the image relying on pre-trained region detectors. The pre-trained detector however prevents the whole pipeline from end-to-end training, whilst any detection errors can directly impair the report generation performance. In addition, many previous methods [4,3,14] supervise the training process of RRG models by adopting similar losses/metrics used for image captioning, consequently, the generated reports often fail to reflect the comprehensive clinical significant and insignificant errors that radiologists would emphasize. For instance, radiologists tend to use many negations in their reports (*e.g.*, “no pneumothorax”) which is a strong difference from natural image captioning.

To address the aforementioned problems, we are inspired by the recent development of large models (LMs) [1,25] and their associated reinforcement learning from human feedback (RLHF) scheme, thereby propose a novel method **LM-driven Chest X-ray Radiology Report Generation with Clinical Quality Reinforcement Learning (CQRL)**, namely **LM-RRG**. It comprises three parts.

The first part is the LLM-driven visual feature extractor, aiming at extracting visual features from different regions of the chest X-ray image, so as to comprehensively cover the medical significance of the image. Inspired by [11,32], we propose to leverage text descriptions of different regions generated by a large language model (LLM, *e.g.*, GPT-4 [1]) to facilitate the visual feature extraction from local regions (*e.g.* left lung, spine) of the chest X-ray image. The second part is the multimodal report generator, designed to generate accurate and comprehensive report from extracted visual features. Benefiting from the inherent strong text generation capabilities of large multimodal models (LMMs) [12,16], we design multimodal prompts that include visual features and textual instruction to guide the decoder of a LMM (*e.g.*, BLIP-2 [12]) for report generation. The multimodal decoder is finetuned with a multitask learning framework including losses for both report generation and disease classification. For the third part, once the model is trained, to further emphasize the clinical significant and insignificant errors in the report, as per radiologists do, we include a feedback loop to reinforce the clinical quality of the generated report, following the similar idea of RLHF [17]. Nevertheless, real radiologist’s feedback is very difficult to achieve in practice, hence a surrogate feedback mechanism is needed. We opt for a metric, radiology reports clinical quality (RadCliQ) [29], which specifically focuses on the clinical (in-/)significant errors in the report. We use it as the reward function in our clinical quality reinforcement learning.

Extensive experiments on the MIMIC-CXR and IU-Xray datasets demonstrate that our method surpasses the state of the art.

## 2 Method

Given a chest X-ray image  $I \in \mathbb{R}^{H \times W \times 3}$ , where  $H$  and  $W$  is the height and width of the image, our method aims to generate the corresponding radiology report  $R$ .

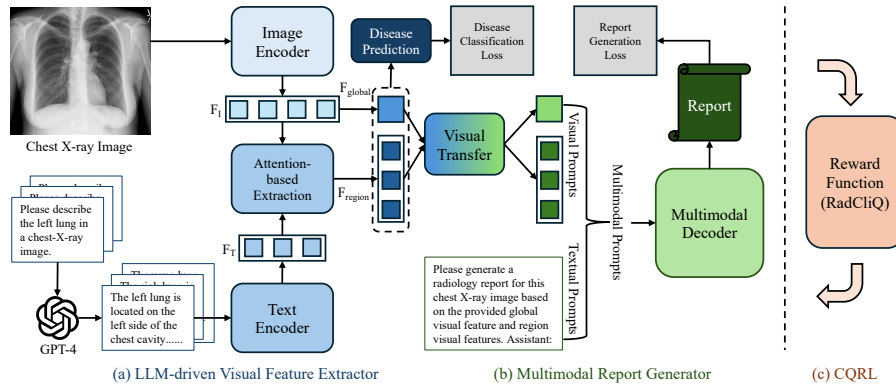


**Fig. 1.** The overall framework of our LM-RRG, which comprises three components: LLM-driven visual feature extractor, multimodal report generator and clinical quality reinforcement learning (CQRL).

As shown in Fig. 1, our method includes three parts: LLM-driven visual feature extractor, multimodal report generator, and reinforcement learning from clinical quality feedback. Below we detail them respectively.

## 2.1 LLM-driven visual feature extractor

To automatically generate radiology reports from chest X-ray images, it is essential to encode the images into visual features corresponding to different regions predefined by radiologists (*e.g.* left lung, mediastinum, spine) [10]. We utilize text descriptions of different regions generated by a pretrained LLM (*e.g.* GPT-4 [1]) to interact with the image (see the supplementary material for generated descriptions). The text descriptions are denoted by  $T \in \{t_k | k = 1, 2, \dots, K\}$  for  $K$  (*i.e.*, 29) different regions. We employ the encoders from a medical CLIP model pre-trained on 2D medical image-text datasets [30]: its text encoder is used to extract the textual feature  $F_T^k \in \mathbb{R}^{1 \times D}$  for each region description  $t_k$ , where  $D$  is the dimension of the feature; its image encoder is used to extract the visual features  $F_I \in \mathbb{R}^{N \times D}$  from the chest X-ray image  $I$ , where  $N$  represents the number of visual tokens. Below, we specify the extraction of the text-prompting visual region features given  $F_I$  and  $F_T^k$ .

**Text-prompting visual region features.** We propose to extract visual region features through a text-prompting way [11,32], novelly avoiding explicit region detection. An attention mechanism is employed to extract the visual region features  $F_{region}^k$  from the visual features  $F_I$  through the guidance of textual features  $F_T^k$ . Initially, we use *cross-attention*, treating  $F_I$  as the query and  $F_T^k$  as both key and value, to facilitate their interaction. This process let  $F_I$  perceive visual information pertinent to the textual information of the corresponding region. It is expressed as:  $F_{CA}^k = CA(LN(F_I), F_T^k) + F_I$ , where  $CA(\cdot)$  represents the cross-attention operation and  $LN(\cdot)$  the layer normalization. Subsequently, we apply a self-attention to  $F_{CA}^k$  for enhancing its region-specific information. This step is

described as:  $F_{SA}^k = SA(LN(F_{CA}^k)) + F_{CA}^k$ , where  $SA(\cdot)$  represents self-attention operation. Finally, we introduce a feed-forward network to encode and further refine  $F_{SA}^k$ , denoted as:  $F_{FFN}^k = FFN(LN(F_{SA}^k)) + F_{SA}^k$ , where  $FFN(\cdot)$  denotes feed-forward network. Note,  $CA(\cdot)$ ,  $SA(\cdot)$ , and  $FFN(\cdot)$  are components within a block, and by repeating this block multiple times (*e.g.* 3), we ultimately obtain  $F_{region}^k \in \mathbb{R}^{1 \times D}$ . By processing all  $K$  regions in parallel and concatenating their outputs, we obtain the final region features  $F_{region} \in \mathbb{R}^{K \times D}$ .

Considering that the image’s global information can also benefit the model for report generation, we extract the global feature. To achieve this, we simply take the average of the  $N$  extracted patch features along the token dimension and obtain the global feature, denoted by  $F_{global} \in \mathbb{R}^{1 \times D}$ .

## 2.2 Multimodal report generator

After extracting visual features  $F_{global}$  and  $F_{region}$ , we aim to enable the multimodal report generator  $G(\cdot)$  to produce accurate and comprehensive radiology report  $R$ . To achieve it, we first construct multimodal prompts, which comprise the global and region features, as well as the instruction to guide the decoder. These multimodal prompts are then fed into a multimodal decoder from a LMM (*e.g.* BLIP-2 [12]), which auto-regressively generates the radiology report.

**Multimodal prompts construction.** The multimodal prompts consist of two components: the visual prompts (global and region features) and the textual prompts (instruction). We need to process them to ensure they can be compatible with the multimodal decoder’s input format.

*Visual prompts.*  $F_{global}$  and  $F_{region}$  cannot be directly fed into the multimodal decoder. Motivated by [12], we construct a visual transfer module  $VTrans(\cdot)$  to transform these features into ones that are feedable into the decoder. Unlike [12], which compresses large number of visual features into a small number through learnable queries, our global and region features are not many, hence do not need to be compressed. Therefore, we employ a standard 3-layer transformer that each layer includes only a self-attention and a feed-forward network as the visual transfer module  $VTrans(\cdot)$ . This module inputs the global and region features and outputs transferred global and region features, formulated as

$$F_{global}^{vtrans}, F_{region}^{vtrans} = VTrans(F_{global}, F_{region}). \quad (1)$$

The input and output dimensions of the features are the same.

*Textual prompts.* For textual prompts, the aim is to ensure the multimodal decoder understands the meaning of the given features and what actions are required based on these features. Following this principle, we construct instruction  $T_{inst}$ , *i.e.* “Please generate a radiology report for this chest X-ray image based on the provided global visual feature and region visual features. Assistant: ”. We then use the tokenizer of the LMM to transform this instruction into features  $F_{inst} \in \mathbb{R}^{L \times D}$ , where  $L$  represents the length of the instruction and  $D$  denotes the feature dimension.

We concatenate the features corresponding to the visual and textual prompts along the token dimension to obtain the multimodal prompts,  $F_{multimodal} \in \mathbb{R}^{(1+K+L) \times D}$ , which are then input into the multimodal decoder.

**Multimodal decoder.** After the construction of the multimodal prompts, we input these prompts into the multimodal decoder  $Decoder(\cdot)$  and adopt an auto-regressive way for the generation of the radiology report  $R$ . Specifically, for the  $i$ -th token  $t_i$  to be generated in the report, prediction is based on the multimodal prompts and all previously generated tokens, expressed as:

$$t_i = Decoder(F_{multimodal}, t_0, \dots, t_{i-1}), i \in \{0, 1, \dots, M\}, \quad (2)$$

where  $M$  is the maximum length of the generated report. The auto-regressive prediction proceeds until the token indicates the end of the report (*i.e.* [EOS]), ultimately yielding the radiology report  $R$ . The multimodal decoder is pretrained from the LMM and is finetuned in a multitask learning framework, see Sec. 2.4.

### 2.3 Clinical quality reinforcement learning

We employ a clinical quality reinforcement learning (CQRL) scheme to further refine the report generator  $G(\cdot)$  after completing the supervised learning as above (see also Sec. 2.4). In the RL process, the parameters of the LLM-driven visual feature extractor  $E(\cdot)$  are frozen.

Using current metrics (*e.g.* BLEU [18]) can not well evaluate the generated report against the significant or insignificant errors written by radiologists. We employ the RadCliQ [29], which serves as a surrogate feedback for the radiologists, as the reward function  $Reward(\cdot)$  in the RL process. It is composed of four metrics BLUE [18], BertScore [31], CheXbert vector similarity [22], and RadGraph F1 [8], and a fitting network over them to achieve the optimum combination. In this way, the achieved RadCliQ can better reflect the clinical relevance between the generated and written reports.

Similar to the proximal policy optimization (PPO) [20] used in RLHF [17], we also use PPO to update model parameters. First, we need to duplicate the report generator  $G(\cdot)$  by creating two versions, one is the reference report generator  $G_{ref}(\cdot)$  whose parameters are frozen, and the other is the model updated through PPO, defined as  $G_{PPO}(\cdot)$ . We employ two losses, the reward loss to improve the model and the KL divergence loss to ensure that the outputs of two models do not diverge significantly.

$$\mathcal{L}_{reward} = -Reward(R, \hat{R}); \quad \mathcal{L}_{KL} = Dist_{KL}(G_{ref}(E(I, T)), G_{PPO}(E(I, T))), \quad (3)$$

where  $Dist_{KL}$  is the operator to calculate the KL distance. Therefore, the total loss for the CQRL is

$$\mathcal{L}_{RL} = \mathcal{L}_{reward} + \lambda_{KL} \mathcal{L}_{KL}, \quad (4)$$

where  $\lambda_{KL}$  is an adaptive weighting coefficient, and is adjusted according to the following formula:

$$\lambda_{KL} = \begin{cases} 1 & Reward(R, \hat{R}) \geq \theta, \\ Reward(R, \hat{R})/\theta & \text{others,} \end{cases} \quad (5)$$

where  $\theta$  acts as a controlling threshold. When the model achieves a reward greater than or equal to  $\theta$ , it indicates that the current generated report is close to the ground truth report. In this case, by setting  $\lambda_{KL} = 1$ , we ensure that the model’s output should be as close as possible to that of the reference model. Conversely, if the gap between the model’s generated report and the ground truth is significant, the loss should be turned to the reward loss.

## 2.4 Model training

There are two learning stages for our method, the first is supervised learning and the second is the reinforcement learning. For the first stage, we employ a multitask learning framework including two losses: the language modeling loss  $\mathcal{L}_{reprot}$  [1] to optimize the generated report, and the disease classification loss  $\mathcal{L}_{disease}$  to equip the visual features with more disease-related information. The former is computed upon the output report while the latter is branched off from the combination of global and region visual features for multi-class prediction (see Fig. 1). Both use the cross-entropy form. The total loss  $\mathcal{L}$  is  $\mathcal{L} = \lambda\mathcal{L}_{disease} + \mathcal{L}_{report}$ . For the second stage, please refer to Sec. 2.3.

## 3 Experiments

### 3.1 Datasets and metrics

**Datasets.** Following previous works [3,4,19], we use the MIMIC-CXR [10] and IU X-Ray [5] datasets to conduct our experiments.

**Metrics.** We utilize metrics such as the Natural Language Generation (NLG), encompassing BLEU [18], METEOR [2], and ROUGE [15]; Clinical Efficacy (CE), including precision, recall, and F1 scores; and Radiology Report Clinical Quality (RadCliQ) [29], which is a composite metric that includes BLEU [18], BERTScore [31], CheXbert vector similarity [22], and RadGraph F1 [8]. Note that for the NLG and CE metrics, higher values indicate better performance, whereas for RadCliQ, lower values signify better results.

### 3.2 Comparison to state of the art

**MIMIC-CXR.** Tab. 1 shows the results of our method compared with previous methods on the MIMIC-CXR dataset. The previous best-performing method on the NLG metrics, *i.e.* COMG [6], also utilizes region features and reinforcement learning, our method beats it clearly, *e.g.* +3.7% on METEOR; furthermore, our method significantly outperforms COMG on the CE metrics, *e.g.* +13.9% on F1. On the other hand, compared to the previous best-performing method on the CE metrics, PromptMRG [9], our method performs on par with it on CE but surpasses it significantly on NLG, *e.g.* +2.8% on ROUGE. In terms of the RadCliQ metric, our method, benefiting from using RadCliQ as the feedback function, shows a substantial improvement over previous methods [4,28]. These results demonstrate the effectiveness of our method.

**Table 1.** Comparison of our method with state of the art on the MIMIC-CXR.

Method	NLG			CE			RadCliQ↓
	BLEU4↑	METEOR↑	ROUGE↑	Precision↑	Recall↑	F1↑	
R2Gen [4]	0.103	0.142	0.277	0.333	0.273	0.276	1.552
WCL [28]	0.107	0.144	0.274	0.385	0.274	0.294	1.511
DCL [13]	0.109	0.150	0.284	0.471	0.352	0.373	–
RGRG [24]	0.126	0.168	0.264	0.461	0.475	0.447	–
UAR [14]	0.107	0.157	0.289	–	–	–	–
PromptMRG [9]	0.112	0.157	0.268	0.501	0.509	0.476	–
COMG [6]	0.124	0.128	0.290	0.424	0.291	0.345	–
<b>LM-RRG(Ours)</b>	0.122	0.165	0.296	0.500	0.500	0.484	0.865

**Table 2.** Comparison of our method with state of the art on the IU-Xray.

Method	NLG		
	BLEU4↑	METEOR↑	ROUGEL↑
DCL [13]	0.163	0.193	0.383
UAR [14]	0.200	0.218	0.405
PromptMRG [9]	0.098	0.160	0.281
COMG [6]	0.206	0.218	0.383
<b>LM-RRG(Ours)</b>	0.208	0.216	0.387

**IU-Xray.** Tab. 2 shows the performance comparison between our method and state of the art. Note that the only the NLG metrics are utilized for this dataset as a default practice. The results of our method are basically on par with the state of the art. Compared to the MIMIC-CXR, the IU-Xray is of much smaller scale and is not the main benchmarking dataset (368,960 vs 7,470). Hence, our hyper-parameters used on MIMIC-CXR are directly applied on IU-Xray.

### 3.3 Ablation study

To validate the effectiveness of each module designed in our method, we conduct ablation study on the MIMIC-CXR dataset.

**LLM-driven visual feature extractor.** We study the impact of global and region visual features, as well as the text prompts for region features.

*Global and region visual features.* To validate the effect of using both global and local visual features, we conduct experiments by respectively removing them from the feature extractor. In Tab. 3, the results show that when global feature is removed (w/o  $F_I^{global}$ ), there is a slight performance decline on all metrics, validating the contribution of the global information to report generation. On the other hand, when we remove the region features (w/o  $F_I^{region}$ ), we observe a more significant decrease on all metrics (*e.g.*-1.0% in Meteor and -3.7% in F1), indicating that region features are crucial for accurate report generation.

*Text prompts for local region features.* To validate the effect of obtaining region descriptions from the LLM to serve as the prompts for extracting region features, we replace them by simply using the region names as prompts. The results in Tab. 3 (descriptions  $\rightarrow$  names) show a clear decrease by doing so. Using only the region names cannot provide sufficient region information for feature extraction, hence proving the necessity of using LLM-produced descriptions.

**Table 3.** Ablation study for LLM-driven visual feature extractor, multimodal report generator and clinical quality reinforcement learning.

Ablation	NLG			CE			RadCliQ↓
	BLEU4↑	METEOR↑	ROUGE↑	Precision↑	Recall↑	F1↑	
LM-RRG	0.122	0.165	0.296	0.496	0.495	0.484	0.865
w/o $F_I^{global}$	0.119	0.158	0.293	0.493	0.489	0.471	0.880
w/o $F_I^{region}$	0.115	0.155	0.291	0.477	0.465	0.447	1.052
text: descriptions → names	0.116	0.154	0.293	0.472	0.468	0.444	1.054
w/o $F_{inst}$	0.119	0.159	0.292	0.484	0.481	0.462	0.906
w/o $\mathcal{L}_{disease}$	0.122	0.164	0.296	0.462	0.461	0.449	0.919
w/o CQRL	0.117	0.167	0.295	0.497	0.493	0.483	1.023
reward: RadCliQ → BLEU4	0.127	0.163	0.291	0.486	0.484	0.471	1.102
w/ fixed $\lambda_{KL}$	0.120	0.164	0.295	0.496	0.493	0.483	0.901

**Multimodal report generator.** To validate the effect of the text instruction in the multimodal report generator, we conduct an experiment by removing it. This (Tab. 3: w/o  $F_{inst}$ ) leads to performance decrease on all metrics (*e.g.*, -2.2% in F1), demonstrating the necessity of the text instruction in the multimodal report generator.

**Multitask learning framework.** Our multitask learning framework consists of two loss, the language modelling loss and the disease classification loss. The former is essential while the latter serves as an auxiliary loss, so we remove the latter to verify its effect (see Tab. 3: w/o  $\mathcal{L}_{disease}$ ). The results show that this leads to a clear performance decrease, *e.g.*-3.5% on F1. The  $\mathcal{L}_{disease}$  proves to be also beneficial to the report generation.

**Clinical quality reinforcement learning.** First, when we omit the CQRL process, in Tab. 3 we find that the model’s RadCliQ performance worsens significantly by 0.158, validating its effectiveness.

*Reward function in RL.* The reward function in the RL can also be of other forms, *e.g.* BLEU4. In the Tab. 3, we find that the model’s BLEU4 performance can improve by 0.5% when we replace RadCliQ with BLEU4, but the results on other metrics significantly decline, suggesting the model is biased during the RL. In contrast, if we compare between w/o CQRL and LM-RRG in Tab. 3, by adding RL with RadCliQ, not only the result on RadCliQ is improved, the results on other metrics are remained or even improved, suggesting an unbiased performance gain by the model.

*Adaptive  $\lambda_{KL}$ .* In the RL learning, if we change the  $\lambda_{KL}$  to a fixed value of 1 (Tab. 3: use fixed  $\lambda_{KL} = 1$ ), it will result in a slight performance decrease, validating the usage of the adaptive  $\lambda_{KL}$ .

## 4 Conclusion

In this work, we present a novel approach LM-RRG that combines LMs with clinical quality reinforcement learning to generate sensible and accurate chest X-ray reports. Our method consists of an LLM-driven visual feature extractor that captures visual features from both specific regions and the entire image; a multimodal report generator that comprises a multimodal prompts constructor



and a multimodal decoder to produce coherent the report using these visual and textual prompts. Additionally, we employ a reinforcement learning mechanism with RadCliQ as the reward function to enhance the clinical accuracy of the generated reports. Our approach surpasses state of the art on the MIMIC-CXR and IU-Xray datasets. Future work will be focused on working with hospitals to apply our method into their systems and refine it accordingly.

**Acknowledgments.** This work was supported by King’s Cambridge 1 Access Fund, Tongji Fundamental Research Funds for the Central Universities, and core funding from the Wellcome/EPSRC [WT203148/Z/16/Z; NS/A000049/1]. Computing resources provided by King’s Computational Research, Engineering and Technology Environment (CREATE). For the purpose of open access, the authors have applied a CC BY public copyright licence to any Author Accepted Manuscript version arising from this submission. TV is supported by a Medtronic / RAEng Research Chair [RCSRF1819\7\34], and is co-founder and shareholder of Hypervision Surgical. MW and OA are supported by the EPSRC CDT [EP/S022104/1].

## References

1. Achiam, J., Adler, S., Agarwal, S., Ahmad, L., Akkaya, I., Aleman, F.L., Almeida, D., Altenschmidt, J., Altman, S., Anadkat, S., et al.: Gpt-4 technical report. arXiv preprint arXiv:2303.08774 (2023)
2. Banerjee, S., Lavie, A.: Meteor: An automatic metric for mt evaluation with improved correlation with human judgments. In: ACL workshop on intrinsic and extrinsic evaluation measures for machine translation and/or summarization. pp. 65–72 (2005)
3. Chen, Z., Shen, Y., Song, Y., Wan, X.: Cross-modal memory networks for radiology report generation. In: ACL. pp. 5904–5914 (2021)
4. Chen, Z., Song, Y., Chang, T.H., Wan, X.: Generating radiology reports via memory-driven transformer. In: EMNLP. pp. 1439–1449 (2020)
5. Demner-Fushman, D., Kohli, M.D., Rosenman, M.B., Shooshan, S.E., Rodriguez, L., Antani, S., Thoma, G.R., McDonald, C.J.: Preparing a collection of radiology examinations for distribution and retrieval. *Journal of the American Medical Informatics Association* **23**(2), 304–310 (2016)
6. Gu, T., Liu, D., Li, Z., Cai, W.: Complex organ mask guided radiology report generation. In: WACV. pp. 7995–8004 (2024)
7. Huang, Z., Zhang, X., Zhang, S.: Kiut: Knowledge-injected u-transformer for radiology report generation. In: CVPR. pp. 19809–19818 (2023)
8. Jain, S., Agrawal, A., Saporta, A., Truong, S.Q., Duong, D.N., Bui, T., Chambon, P., Zhang, Y., Lungren, M.P., Ng, A.Y., et al.: Radgraph: Extracting clinical entities and relations from radiology reports. arXiv preprint arXiv:2106.14463 (2021)
9. Jin, H., Che, H., Lin, Y., Chen, H.: Promptmrg: Diagnosis-driven prompts for medical report generation. arXiv preprint arXiv:2308.12604 (2023)
10. Johnson, A.E., Pollard, T.J., Berkowitz, S.J., Greenbaum, N.R., Lungren, M.P., Deng, C.y., Mark, R.G., Horng, S.: Mimir-cxr, a de-identified publicly available database of chest radiographs with free-text reports. *Scientific data* **6**(1), 317 (2019)

11. Kirillov, A., Mintun, E., Ravi, N., Mao, H., Rolland, C., Gustafson, L., Xiao, T., Whitehead, S., Berg, A.C., Lo, W.Y., et al.: Segment anything. arXiv preprint arXiv:2304.02643 (2023)
12. Li, J., Li, D., Savarese, S., Hoi, S.: Blip-2: Bootstrapping language-image pre-training with frozen image encoders and large language models. arXiv preprint arXiv:2301.12597 (2023)
13. Li, M., Lin, B., Chen, Z., Lin, H., Liang, X., Chang, X.: Dynamic graph enhanced contrastive learning for chest x-ray report generation. In: CVPR. pp. 3334–3343 (2023)
14. Li, Y., Yang, B., Cheng, X., Zhu, Z., Li, H., Zou, Y.: Unify, align and refine: Multi-level semantic alignment for radiology report generation. In: ICCV. pp. 2863–2874 (2023)
15. Lin, C.Y.: Rouge: A package for automatic evaluation of summaries. In: Text summarization branches out. pp. 74–81 (2004)
16. Liu, H., Li, C., Wu, Q., Lee, Y.J.: Visual instruction tuning. *Advances in neural information processing systems* **36** (2024)
17. Ouyang, L., Wu, J., Jiang, X., Almeida, D., Wainwright, C., Mishkin, P., Zhang, C., Agarwal, S., Slama, K., Ray, A., et al.: Training language models to follow instructions with human feedback. *NeurIPS* pp. 27730–27744 (2022)
18. Papineni, K., Roukos, S., Ward, T., Zhu, W.J.: Bleu: a method for automatic evaluation of machine translation. In: *ACL*. pp. 311–318 (2002)
19. Qin, H., Song, Y.: Reinforced cross-modal alignment for radiology report generation. In: *Findings of ACL*. pp. 448–458 (2022)
20. Schulman, J., Wolski, F., Dhariwal, P., Radford, A., Klimov, O.: Proximal policy optimization algorithms. arXiv preprint arXiv:1707.06347 (2017)
21. Sharma, H., Agrahari, M., Singh, S.K., Firoj, M., Mishra, R.K.: Image captioning: a comprehensive survey. In: *PARC*. pp. 325–328. *IEEE* (2020)
22. Smit, A., Jain, S., Rajpurkar, P., Pareek, A., Ng, A.Y., Lungren, M.P.: Chexbert: combining automatic labelers and expert annotations for accurate radiology report labeling using bert. arXiv preprint arXiv:2004.09167 (2020)
23. Stefanini, M., Cornia, M., Baraldi, L., Cascianelli, S., Fiameni, G., Cucchiara, R.: From show to tell: A survey on deep learning-based image captioning. *IEEE transactions on pattern analysis and machine intelligence* **45**(1), 539–559 (2022)
24. Tanida, T., Müller, P., Kaissis, G., Rueckert, D.: Interactive and explainable region-guided radiology report generation. In: CVPR. pp. 7433–7442 (2023)
25. Touvron, H., Martin, L., Stone, K., Albert, P., Almahairi, A., Babaei, Y., Baid, A., Baevski, N., Baheti, S., Badra, S., et al.: Llama 2: Open foundation and fine-tuned chat models. arXiv preprint arXiv:2307.09288 (2023)
26. Wang, J., Bhalerao, A., He, Y.: Cross-modal prototype driven network for radiology report generation. In: *ECCV*. pp. 563–579. Springer (2022)
27. Wang, Z., Liu, L., Wang, L., Zhou, L.: Metransformer: Radiology report generation by transformer with multiple learnable expert tokens. In: CVPR. pp. 11558–11567 (2023)
28. Yan, A., He, Z., Lu, X., Du, J., Chang, E., Gentili, A., McAuley, J., Hsu, C.N.: Weakly supervised contrastive learning for chest x-ray report generation. arXiv preprint arXiv:2109.12242 (2021)
29. Yu, F., Endo, M., Krishnan, R., Pan, I., Tsai, A., Reis, E.P., Fonseca, E.K.U.N., Lee, H.M.H., Abad, Z.S.H., Ng, A.Y., et al.: Evaluating progress in automatic chest x-ray radiology report generation. *Patterns* **4**(9) (2023)

30. Zhang, S., Xu, Y., Usuyama, N., Xu, H., Bagga, J., Tinn, R., Preston, S., Rao, R., Wei, M., Valluri, N., Wong, C., Tupini, A., Wang, Y., Mazzola, M., Shukla, S., Liden, L., Gao, J., Lungren, M.P., Naumann, T., Wang, S., Poon, H.: Biomedclip: a multimodal biomedical foundation model pretrained from fifteen million scientific image-text pairs (2024)
31. Zhang, T., Kishore, V., Wu, F., Weinberger, K.Q., Artzi, Y.: Bertscore: Evaluating text generation with bert. arXiv preprint arXiv:1904.09675 (2019)
32. Zhou, Z., Alabi, O., Wei, M., Vercauteren, T., Shi, M.: Text promptable surgical instrument segmentation with vision-language models. NeurIPS (2024)

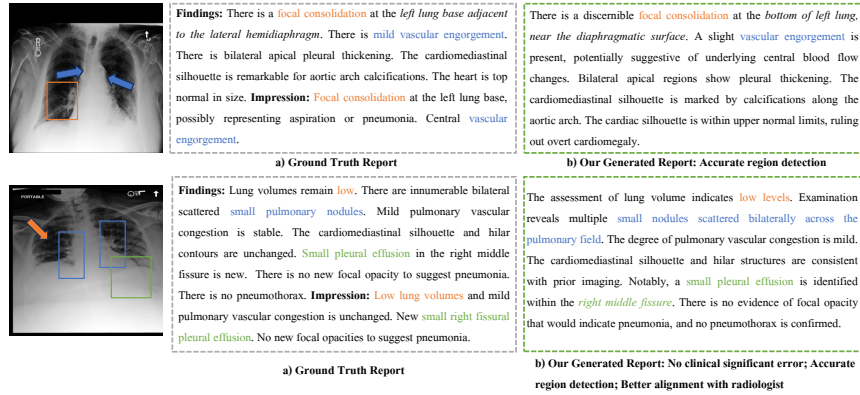


**Fig. 2.** Two examples of our generated reports, alongside their input radiology images and ground truth reports. Critical findings in the radiology images are roughly labelled (denoted in coloured boxes); The clinical significant/insignificant observations are highlighted in both reports; a) Illustration of the ground truth report, including critical findings and the impression annotated by radiologists. b) Report generated by our LM-CQRL. Our reports accurately identify the regions of abnormalities and closely align with the ground truth.

**Region description from GPT-4.** There are 29 different regions defined in MIMIC-CXR. They are generated by asking LLM (GPT-4), *i.e.*, “Please description the {region name} in a chest X-ray image, and summarize it.”. Due to page limitations, we only provide descriptions for 12 regions.

- *Left lung*: The left lung presents as a transparent area with two lobes, bordered by the ribcage, extending from collarbone to diaphragm, adjacent to the heart’s left border, showing clear fields without opacities, masses, or fluid levels, indicating normal pulmonary status.
- *Right lung*: The right lung, larger than the left, spans from collarbone to diaphragm, enclosed by the ribcage, divided into three lobes by distinct fissures, and displays clear, transparent lung fields without abnormalities, ensuring a healthy pulmonary condition adjacent to the heart’s edge.
- *Cardiac silhouette*: The cardiac silhouette on a chest X-ray, appearing as a centrally located, denser area with smooth contours, occupies less than half of the thoracic width on the left side, providing insights into the heart’s condition through its shape and size, indicative of the individual’s normal cardiac health when aligned with expected standards for their body size and age.
- *Mediastinum*: The mediastinum is visible as the central thoracic compartment with varied densities, housing critical structures between the lungs, marked by well-centered positioning, clear margins, and standard width; its normal appearance—free from widening, mass effects, or shifts—indicates the absence of underlying pathology and maintains thoracic health.

- *Right hilar structures*: The right hilar structures, comprising bronchi, blood vessels, lymph nodes, and nerves, are centrally positioned on the right side, slightly higher than the left, displaying clear and defined edges without enlargement or abnormal shadows, indicating normal pulmonary and vascular health when devoid of disease indicators.
- *Upper mediastinum*: The upper mediastinum appears above the heart level, delineated by well-defined, smooth contours housing the trachea and major vessels; its normal state—without undue widening, masses, or abnormal densities—suggests the absence of pathologies like lymphadenopathy or tumors, reflecting healthy thoracic anatomy and function.
- *Left costophrenic angle*: The left costophrenic angle, formed by the intersection of the diaphragm and left rib cage, appears as a sharp, clear space at the lung's lower edge, crucial for evaluating pleural space and lung health; its well-defined visibility without blunting or fluid levels signals no pleural effusion, reflecting normal pulmonary status.
- *Aortic arch*: The aortic arch manifests as a smooth, convex curve atop the heart's left side, part of the upper mediastinal silhouette, with its distinct contour without widening or irregularities indicative of cardiovascular health; abnormalities like aneurysms or calcifications signal potential issues, making its clear visibility crucial for assessing aortic and overall cardiac conditions.
- *Right hemidiaphragm*: The right hemidiaphragm, delineated by a smooth, dome-shaped line above the liver, typically sits higher than its left counterpart, showcasing uninterrupted contours essential for evaluating diaphragmatic integrity, respiratory function, and potential subdiaphragmatic issues, with normal appearance indicating healthy pulmonary and abdominal regions.
- *Right clavicle*: The right clavicle is displayed as a smooth, curved bone at the thorax's top, symmetrical with the left but positioned on the image's right side; its intact, uniform appearance without breaks or deformities is crucial for assessing shoulder and thoracic area integrity, indicating normal skeletal health and serving as a vital anatomical landmark.
- *Trachea*: The trachea appears as a central, tubular, and slightly curved structure with clear, parallel walls, extending from below the neck to the bronchial bifurcation; its straight alignment and unobstructed appearance without deviation, narrowing, or obstruction signify healthy airway passages and absence of thoracic pathologies, crucial for respiratory function assessment.
- *Spine*: The spine appears as a straight, central column of increasing-sized rectangular vertebrae, properly aligned without misalignment or fractures, behind heart and mediastinal structures; uniform disc spaces without narrowing indicate the absence of degenerative changes, essential for assessing spinal integrity and overall thoracic health.